Dynamic Characteristics of a DC Motor Controlled by Single-Phase Half-Wave Thyristor Rectifier Circuit

AUTHOR(S):

ANDŌ, Tsuguo; UMOTO, Jūrō

Dynamic Characteristics of a DC Motor Controlled by Single-Phase Half-Wave Thyristor Rectifier Circuit

By

Tsuguo ANDŌ* and Jūrō UMOTO*

(Received September 30, 1971)

When the armature voltage of a dc motor is being controlled by a thyristor rectifier circuit, the armature current sometimes flows discontinuously. In this paper, the authors analyse the dynamic characteristics of a separately excited dc motor controlled by the single-phase half-wave thyristor rectifier circuit and investigate the influence of the discontinuous current on the motor performances. Considering the small fluctuation of the motor speed during one cycle of the ac source frequency and the friction torque of the motor, they develop a theoretical analysis of the motor performance and from the result they deduce a graphical method, by which the performance can be easily analysed. Then they compare the theoretical results with experimental ones and investigate quantitatively the effects of the circuit parameters on the dynamic performance of the motor.

1. Introduction

In recent years, many reports of application of dc motors have been published, of which the armature powers are controlled by thyristor rectifier circuits. However, the analysis of the motor performances has been mostly carried out under the assumption that the fluctuation of the motor speed is negligible[1),2)], and papers that dealt with the dynamic characteristics considering the fluctuation are rarely found[3)]. Also in order to improve still more the control characteristic of the motor, the exact analysis of the dynamic and the static performance has been desired.

Now in this paper the authors develope a theoretical method to analyse the dynamic characteristics of a separately excited dc motor controlled by a single-phase half-wave thyristor rectifier circuit, in which the armature current flows discontinuously, by using the analytical method of periodically interrupted electric circuits[4)]. In their analysis, the fluctuation of the motor speed and the friction torques of the motor with load are considered, which have not been considered in the conventional analyses. Next they introduce a graphical method, by which the dynamic characteristics can be easily analysed.

* Department of Electrical Engineering.

Also the authors compare the calculated results with the experimental ones and confirm the appropriateness of their theory, and from their results they also give some suggestions to the analysis of the speed control of a dc motor by the thyristor circuit.

Here, though the motor is usually controlled by a polyphase rectifier to reduce the ripples of the armature current, the armature current sometimes flows discontinuously, if the armature circuit inductance or the motor load is small. Then the dynamic characteristics of the motor are different from the case of the continuous current. So in order to investigate the influences of the discontinuous current on the motor performance, the authors use a half-wave rectifier circuit.

2. Control Circuit and Operational Modes

Fig. 1 shows the circuit diagram of a single-phase half-wave thyristor rectifier circuit for the speed control of the separately excited dc motor, of which the armature voltage is controlled by changing the firing angle of the thyristor T_h. In the figure,

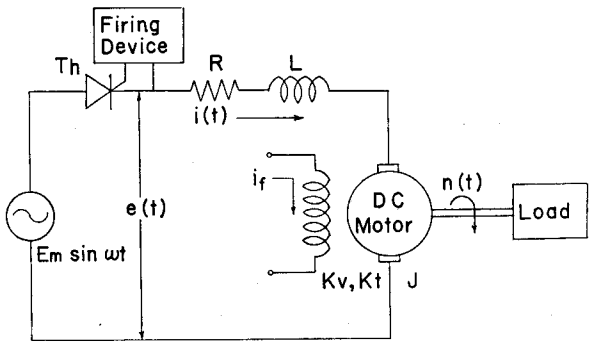

Fig. 1. Control circuit of separately excited dc motor.

$E_m \sin \omega t$: ac source voltage ($\omega = 2\pi f$),
f : ac source frequency,
$e(t)$: terminal voltage of armature circuit,
$i(t)$: armature current,
$n(t)$: motor speed,
t : time,
i_f : fixed field current of motor,
L : total inductance in armature circuit,
R : total resistance in armature circuit,

K_v : counter emf coefficient of motor,

K_t : torque coefficient of motor,

J : moment of inertia of motor with load.

Now there are three types of friction torques to be considered in the analysis of the dc motor with load, namely, static, coulomb and viscous friction torques. The static torque Q_s is the one which is needed to rotate a stalled motor. The coulomb torque Q is the one that exists in a rotating motor and is independent of the speed. The viscous torque is the one which is approximately proportional to the first power of the speed and expressed by $F\ n(t)$, where F is the viscous friction coefficient. Fig. 2 illustrates the relation of the friction torques vs. the motor speed.

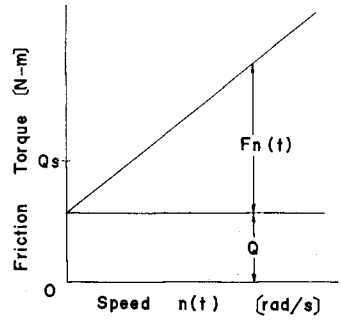

Fig. 2. Approximate speed-torque characteristic.

Next let us consider the circuit operations in Fig. 1. The current $i(t)$ begins to flow at the instant when T_h is fired, and the driving torque $K_t i(t)$ is added to the motor. On the other hand the stalled motor begins to rotate when $K_t i(t)$ exceeds Q_s. When $i(t)$ decreases to zero, $i(t)$ is blocked by a reverse blocking characteristic of T_h and the motor rotates by inertia. But when the average value of $K_t i(t)$ is smaller than Q the motor can't keep rotating and rests.

Therefore we can divide the circuit operations into the four fundamental modes, depending of the situations of $i(t)$ and $n(t)$, as follows:

mode 1 : $i(t)$ is zero and the motor is at rest,

mode 2 : motor can't rotate because lack of torque which is generated by $i(t)$,

mode 3 : motor is driven by $i(t)$

mode 4 : $i(t)$ is blocked and the motor is rotated by inertia.

The situations of $i(t)$ and $n(t)$ in each mode and the criteria for the mode transitions are shown in Fig. 3, where

$I_s = Q_s/K_t$: equavilent constant current for Q_s,

$v(t) = K_v n(t)$: counter emf of motor,

α : firing angle of thyristor.

3. Electrical Equivalent Circuit and Analysis of Mode

Although the circuit operations of the electromechanical system in Fig. 1 can be analysed by considering each mode shown in Fig. 3, where in order to simplify the circuit analysis we use the electrical equivalent circuits.

Now as we can make the forced current source and the terminal voltage of a capacitance correspond to the coulomb torque and the counter emf of the motor respectively, the electrical equivalent circuits for modes 1 to 4 are as shown in Fig.s 4(a) to (d). But in Fig.s 4(a) to (d) and in the following analyses

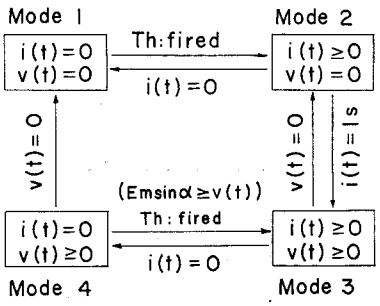

Fig. 3. Operation modes.

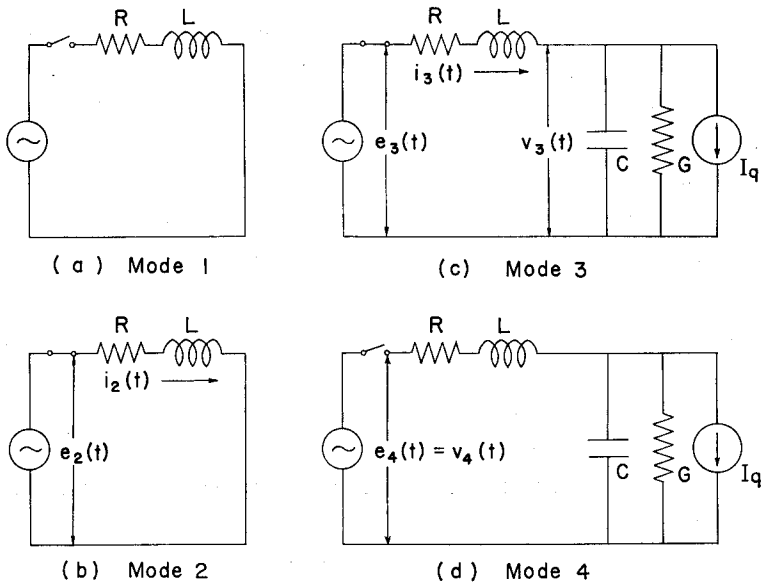

Fig. 4. Electrical equivalent circuits for modes 1 to 4.

$C=J/(K_v K_t)$: equivalent capacitance for J,
$G=F/(K_v K_t)$: equivalent conductance for F,
$I_q=Q/K_t$: equivalent forced current for Q,
$E_{dr}=\frac{1}{\tau}\int_0^{t_r} e_r(t)\,dt$: average voltage of $e_r(t)$,
$I_{dr}=\frac{1}{\tau}\int_0^{t_r} i_r(t)\,dt$: average current of $i_r(t)$,
$V_{dr}=\frac{1}{\tau}\int_0^{t_r} v_r(t)\,dt$: average voltage of $v_r(t)$,
t_r : duration of interval of mode r,
r : mode number,
$\tau=1/f=2\pi/\omega$: period of ac source frequency.

Also we neglect the forward voltage drop in the thyristor T_h and the nonlinearlities of the circuit parameters.

3.1 Mode 1.

From Fig. 4(a) we can readily arrive at the following equations

$$\left.\begin{aligned} &e_1(t)=i_1(t)=v_1(t)=0\,,\\ &E_{d1}=I_{d1}=V_{d1}=0\,. \end{aligned}\right\} \tag{1}$$

3.2 Mode 2.

In Fig. 4(b), assuming that mode 2 starts at the phase angle α_2, we have

$$\left.\begin{aligned} e_2(t) &= E_m \sin(\omega t+\alpha_2)\\ &= L\,d\,i_2(t)/dt + R\,i_2(t)\,,\\ v_2(t) &= 0\,. \end{aligned}\right\} \tag{2}$$

Solving Eq.s (2), we obtain

$$i_2(t)=\varphi_2(t)+\chi_2(t)\,i_2{}^{+0}\,, \tag{3}$$

where

$$\varphi_2(t)=\frac{E_m}{\sqrt{R^2+\omega^2L^2}}\{\sin(\omega t+\alpha_2-\delta)-\chi_2(t)\sin(\alpha_2-\delta)\}\,,$$

$$\chi_2(t)=\varepsilon^{-\frac{R}{L}t}\,,$$

$$\delta=\tan^{-1}(\omega L/R)\,,$$

$i_2{}^{+0}$: initial value of $i_2(t)$.

Next integrating Eq.s (2) from $t=0$ to t_2, the average values E_{d2}, I_{d2} and V_{d2}

become

$$\left.\begin{aligned} E_{d2} &= \frac{E_m}{2\pi}\{\cos\alpha_2 - \cos(\omega t_2 + \alpha_2)\}\,, \\ I_{d2} &= \frac{1}{R}\left[E_{d2} - \frac{L}{\tau}\{i_2(t) - i_2{}^{+0}\}\right], \\ V_{d2} &= 0\,, \end{aligned}\right\} \tag{4}$$

where t_2 is obtained by $i_2(t_2)=0$ or $i_2(t_2)=I_s$.

3.3 Mode 3.

The circuit equations for Fig. 4(c) are given by

$$\left.\begin{aligned} e_3(t) &= E_m \sin(\omega t + \alpha_3) \\ &= L\,di_3(t)/dt + Ri_3(t) + v_3(t)\,, \\ i_3(t) &= C\,d\,v_3(t)/dt + G\,v_3(t) + I_q\,, \end{aligned}\right\} \tag{5}$$

where α_3 is the starting phase angle of mode 3. Solving Eq. (5) we can obtain the solutions in the matrix notation

$$\begin{bmatrix} i_3(t) \\ v_3(t) \end{bmatrix} = \begin{bmatrix} \varphi_{31}(t) \\ \varphi_{32}(t) \end{bmatrix} + \begin{bmatrix} \chi_{311}(t) & \chi_{312}(t) \\ \chi_{321}(t) & \chi_{322}(t) \end{bmatrix} \begin{bmatrix} i_3{}^{+0} \\ v_3{}^{+0} \end{bmatrix}, \tag{6}$$

where

$$\begin{aligned} \varphi_{31}(t) &= I_m\{\sin(\omega t + \alpha_3 + \theta_1 - \theta_2) - \chi_{311}(t)\sin(\alpha_3 + \theta_1 - \theta_2)\} \\ &\quad - V_m\,\chi_{312}(t)\sin(\alpha_3 - \theta_2) + I_q\{1 - g_3(t)\}/(RG+1)\,, \\ \varphi_{32}(t) &= V_m\{\sin(\omega t + \alpha_3 - \theta_2) - g_3(t)\sin(\alpha_3 - \theta_2) \\ &\quad - \omega g_2(t)\cos(\alpha_3 - \theta_2)\} - I_q\,[\chi_{321}(t) + R \\ &\quad \times \{1 - g_3(t)\}/(RG+1)]\,, \\ \chi_{311}(t) &= g_1(t) - \sigma g_2(t)\,, \quad \chi_{312}(t) = -g_2(t)/L\,, \\ \chi_{321}(t) &= g_2(t)/C\,, \quad \chi_{322}(t) = g_1(t) + \sigma g_2(t)\,, \\ g_1(t) &= \varepsilon^{-\lambda t}\cosh\mu t\,, \quad g_2(t) = \varepsilon^{-\lambda t}\sinh\mu t/\mu \text{ for } \sigma^2 LC > 1\,, \\ g_1(t) &= \varepsilon^{-\lambda t}\,, \quad g_2(t) = t\varepsilon^{-\lambda t} \text{ for } \sigma^2 LC = 1\,, \\ g_1(t) &= \varepsilon^{-\lambda t}\cos\mu t\,, \quad g_2(t) = \varepsilon^{-\lambda t}\sin\mu t/\mu \text{ for } \sigma^2 LC < 1\,, \\ g_3(t) &= g_1(t) + \lambda g_2(t)\,, \\ V_m &= E_m/\{(RG + 1 - \omega^2 LC)^2 + \omega^2(LG + CR)^2\}^{1/2}\,, \\ I_m &= (G^2 + \omega^2 C^2)^{1/2} V_m\,, \quad \theta_1 = \tan^{-1}(\omega C/G)\,, \\ \theta_2 &= \tan^{-1}\{\omega(LG + CR)/(RG + 1 - \omega^2 LC)\}\,, \\ \lambda &= (R/L + G/C)/2\,, \quad \sigma = (R/L - G/C)/2\,, \end{aligned}$$

$\mu = |\sigma^2 - 1/(LC)|^{1/2}$,

i_3^{+0} : initial value of $i_3(t)$,

v_3^{+0} : initial value of $v_3(t)$.

Now integrating Eq.s (4) from $t=0$ to t_3, where t_3 can be determined by $i_3(t_3)=0$ or $v_3(t_3)=0$, E_{d3}, I_{d3} and V_{d3} are shown by

$$\left.\begin{aligned} E_{d3} &= \frac{E_m}{2\pi}\{\cos\alpha_3 - \cos(\omega t_3 + \alpha_3)\} , \\ I_{d3} &= G V_{d3} + \frac{t_3}{\tau} I_q + \frac{C}{\tau}\{v_3(t_3) - v_3^{+0}\} , \\ V_{d3} &= \frac{1}{RG+1}\left[E_{d3} - \frac{t_3}{\tau} R I_q - \frac{L}{\tau}\{i_3(t_3) - i_3^{+0}\}\right. \\ &\quad \left. - \frac{CR}{\tau}\{v_3(t_3) - v_3^{+0}\}\right] . \end{aligned}\right\} \tag{7}$$

3.4 Mode 4.

The circuit equations for Fig. 4(d) are given by

$$\left.\begin{aligned} e_4(t) &= v_4(t) , \\ i_4(t) &= 0 , \\ 0 &= C\, d\, v_4(t)/dt + G\, v_4(t) + I_q . \end{aligned}\right\} \tag{8}$$

Solving Eq. (8), we get

$$v_4(t) = \varphi_4(t) + \chi_4(t)\, v_4^{+0} , \tag{9}$$

where

$$\varphi_4(t) = \{\chi_4(t) - 1\}\, I_q/G ,$$

$$\chi_4(t) = \varepsilon^{-\frac{G}{C}t} ,$$

v_4^{+0} : initial value of $v_4(t)$.

Next, the average voltages E_{d4} and V_{d4} are given by

$$E_{d4} = V_{d4} = \frac{-1}{\tau G}[t_4 I_q + C\{v_4(t_4) - v_4^{+0}\}] . \tag{10}$$

4. Analysis of Dynamic Characteristics

The dynamic characteristics of the electromechanical system in Fig. 1 can be explained by analysing the circuit performances during any one cycle of the ac

source frequency. Refering to Fig. 3, we can think of the following cases concerning the circuit performance during one cycle

case 1 : motor does'nt rotate,

case 2 : motor, which rests, begins to rotate,

case 3 : motor rotates continuously,

case 4 : motor, which is rotating, stops.

Fig.s 5 (a) to (d) show the illustrative waveforms of $e(t)$, $i(t)$ and $v(t)$ for cases 1 to 4 respectively, where

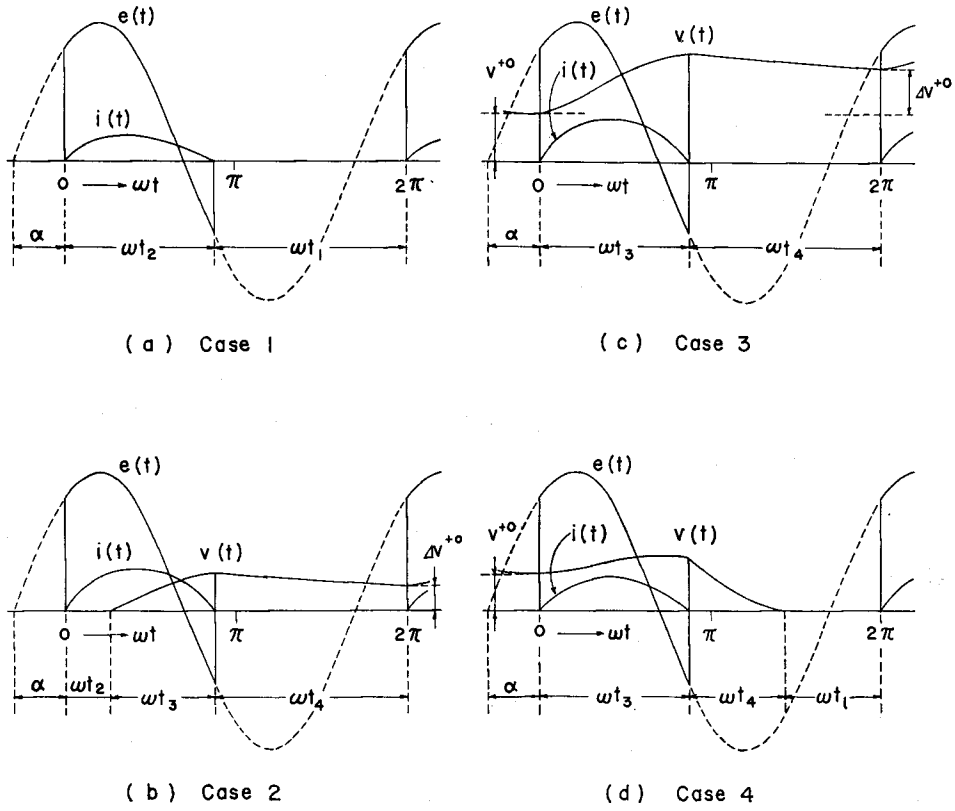

Fig. 5. Illustrative waveformes of $e(t)$, $i(t)$ and $u(t)$ in cases 1 to 4.

α : firing angle of thyristor T_h,

v^{+0} : initial value of $v(t)$, when T_h is fired,

Δv^{+0} : variation of $v(t)$ during any one cycle,

t_r : duration of interval of made r.

$r=1$ to 4 : mode number.

In addition to Fig.s 5(a) to (d), we can consider several mode transitions from Fig. 3.

Now in our system the armature current $i(t)$ can't flow continuously, and so the rough characteristics on the transient and steady state can be secured by finding the sign of Δv^{+0}, namely:

When $\Delta v^{+0}>0$, motor is being accelerated,

When $\Delta v^{+0}=0$, motor reaches steady state,

When $\Delta v^{+0}<0$, motor is being decelerated.

In this section let us introduce the method analysing the dynamic characteristics. But on account of space consideration, as examples, we will show the analysing methods of the characteristics in three cases as shown in Fig.s 5 (a), (b) and (c).

4.1 Case 1.

In this case, the circuit operation during any cycle is determined by modes 2 and 1 as shown in Fig. 5(a). In mode 2, $e(t)$ and $i(t)$ are obtained by substituting $\alpha_2=\alpha$ and $i_2{}^{+0}=0$ into Eq.s (2) and (3). Next putting $i(t_2)=0$, that is $\varphi_2(t_2)=0$, we can get the duration t_2, and then from Eq.s (4) the average values E_d and I_d of $e(t)$ and $i(t)$ respectively are found as

$$\left.\begin{aligned} E_d &= \frac{E_m}{2\pi}\{\cos\alpha - \cos(\omega t_2 + \alpha)\}\,, \\ I_d &= E_d/R\,. \end{aligned}\right\} \tag{11}$$

4.2 Case 2

As shown in Fig. 5(b) the circuit operation is composed of modes 2, 3 and 4. Hence we can easily find the expressions $e(t)$, $i(t)$ and $v(t)$ from Eq. s (2) and (3) for mode 2, Eq.s (5) and (6) for mode 3, and Eq.s (8) and (9) for mode 4. The durations t_2, t_3 and t_4 are determined by

$$\left.\begin{aligned} &\varphi_2(t_2) = I_s\,, \\ &\varphi_{31}(t_3) + \varkappa_{311}(t_3)\, I_s = 0\,, \\ &t_4 = \tau - t_2 - t_3\,. \end{aligned}\right\} \tag{12}$$

Furthermore the average values E_d, I_d and V_d of $e(t)$, $i(t)$ and $v(t)$ are derived from Eq.s (4), (7) and (10).

Now the voltage $v(\tau)$ after lapse of one cycle is given by

$$v(\tau) = \varphi_4(t_4) + \varkappa_4(t_4)\,\{\varphi_{32}(t_3) + \varkappa_{321}(t_3)\, I_s\}\,. \tag{13}$$

Since $v(\tau)$ becomes the initial voltage in the following cycle, the circuit operation is as shown in Fig. 5(c).

4.3 Case 3.

In this case, the circuit operation is represented usually by modes 3 and 4, as shown in Fig. 5(c). In mode 3, $e(t)$, $i(t)$ and $v(t)$ can be obtained by substituting $\alpha_3=\alpha$, $i_3{}^{+0}=0$ and $v_3{}^{+0}=v^{+0}$ into Eq.s (5) and (6). Then the relation between v^{+0} and t_3 is obtained by putting $i(t_3)=0$, namely

$$\varphi_{31}(t_3) + \varkappa_{312}(t_3)\, v^{+0} = 0 \tag{14}$$

Next in mode 4, $v(t)$ is given by substituting $v(t_3)$ and $t-t_3$ for $v_4{}^{+0}$ and t in Eq. (9), respectively. Therefore the voltage $v(\tau)$ and the variation Δv^{+0} are given by

$$\left.\begin{aligned} v(\tau) &= \varphi_4(t_4) + \varkappa_4(t_4)\,\{\varphi_{32}(t_3) + \varkappa_{322}(t_3)\, v^{+0}\}\,, \\ \Delta v^{+0} &= v(\tau) - v^{+0}\,, \end{aligned}\right\} \tag{15}$$

and $v(\tau)$ becomes the initial voltage in the next cycle.

However, in the case of $v^{+0} > E_m \sin\alpha$, the thyristor can't be fired and the circuit operation is represented by mode 4 only. Accordingly $v(\tau)$ and Δv^{+0} are given by substituting $t_3=0$ and $t_4=\tau$ into Eq.s (15).

Now in the steady state where Δv^{+0} becomes zero, the relations between t_3, t_4 and $v_\infty{}^{+0}$ are given by

$$\left.\begin{aligned} &\{\varphi_4(t_4) + \varkappa_4(t_4)\,\varphi_{32}(t_3)\}\,\varkappa_{312}(t_3) = \{\varkappa_4(t_4)\,\varkappa_{322}(t_3) - 1\}\,\varphi_{31}(t_3)\,, \\ &t_3 + t_4 = \tau\,, \\ &v_\infty{}^{+0} = -\varphi_{31}(t_3)/\varkappa_{312}(t_3) \quad : \quad \text{initial voltage in the steady state.} \end{aligned}\right\} \tag{16}$$

Next, the average values E_d, I_d and V_d are obtained from Eq.s (7) and (10), as follows:

$$\left.\begin{aligned} E_d &= \frac{E_m}{2\pi}\{\cos\alpha - \cos(\omega t_3 + \alpha)\} - \frac{1}{\tau G}\,[t_4 I_q + C\,\{v_\infty{}^{+0} - v(t_3)\}]\,, \\ I_d &= G V_d + I_q\,, \\ V_d &= (E_d - R I_q)/(RG+1) = E_d - R I_d\,. \end{aligned}\right\} \tag{17}$$

5. Graphical Analysis of Dynamic Performance

When the dc motor is driven by the dc source voltage, under the assumption of $J/F \gg L/R$, the transfer function $G(s)$ of the motor is usually expressed by[5),6)]

$$G(s) = \frac{v(s)}{e(s)} = \frac{K_d}{s T_d + 1}\left\{1 - \frac{R I_q}{s e(s)}\right\}, \tag{18}$$

where

$$K_d = \frac{K_v K_t}{RF + K_v K_t} = \frac{1}{RG+1}: \text{ gain,}$$

$$T_d = \frac{JR}{RF + K_v K_t} = \frac{CR}{RG+1}: \text{ time constant of the motor,}$$

$e(s)$: s-function of $e(t)$,

$v(s)$: s-function of $v(t)$,

s : Laplace operator.

Then the expression of $v(t)$ is easily obtained by the inverse Laplace transformation of $v(s)$ in Eq. (18).

However, since the armature current flows discontinuously in our circuit, the expression of $v(t)$ becomes very complex as described in the previous section. So let us introduce a graphical method, by which we can analyse the dynamic performance theoretically.

Now we assume that the relations between the initial value v^{+0} of $v(t)$ and its variation Δv^{+0} during one cycle are represented by the curves as shown in Fig. 6 for the various firing angles α_1, α_2, ...

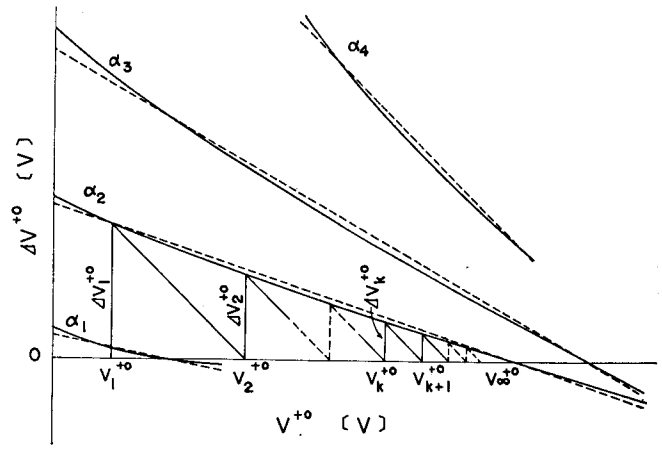

Fig. 6. Illustrative relation between v^{+0} and Δv^{+0}.

Next let us dicuss the process of the change of v^{+0} in the case where the firing angle is α_2 in Fig. 6. When we express the initial value and the variation of $v(t)$ in the first cycle by $v_1{}^{+0}$ and $\Delta v_1{}^{+0}$ respectively, the initial voltage $v_2{}^{+0}$ in the next cycle is given by $v_2{}^{+0}=v_1{}^{+0}+\Delta v_1{}^{+0}$. Repeating a similar treatment, the initial value finally is should arrive at the one $v_\infty{}^{+0}$ in the steady state.

Approximating the $v^{+0}-\Delta v^{+0}$ curves by the dotted straight lines as shown in Fig. 6, the above mentioned process is simplified and the following linear difference equations

$$\left.\begin{aligned} v_{k+1}{}^{+0} &= v_k{}^{+0} + \Delta v_k{}^{+0}\,, \\ \Delta v_k{}^{+0} &= \Delta v_1{}^{+0} - m\,(v_k{}^{+0} - v_1{}^{+0})\,, \end{aligned}\right\} \tag{19}$$

where

$m = -\,d\,\Delta\,v^{+0}/d\,v^{+0}$,

$k = 1, 2, \ldots\ldots,$

$v_k{}^{+0}$ and $\Delta v_k{}^{+0}$: initial value and variation of $v(t)$ in the k-th cycle,

are obtained. Solving Eq.s (19), we can obtain

$$v_{k+1}{}^{+0} = v_\infty{}^{+0}\,\{1 - (1 - m)^k\} + v_1{}^{+0}\,(1 - m)^k\,, \tag{20}$$

where

$0<m<2$: convergence condition of $v_k{}^{+0}$ when k tends to infinity,

$v_\infty{}^{+0} = \lim_{k\to\infty} v_k{}^{+0} = v_1{}^{+0} + \Delta v_1{}^{+0}/m\,.$

Looking for the value of k in the condition of $|\,(1-m)^k\,| \leq \varepsilon^{-1}$, where the term $(1-m)^k$ is the transient one in Eq. (20), the time constant T of the motor is determined by

$$T = k_T\,\tau\,, \tag{21}$$

where

$$\begin{aligned} &k_T = k \geq -\,1/\ln|\,1 - m\,| \quad \text{for} \quad 0 < m < 1 \text{ or } 1 < m < 2\,, \\ &k_T = k = 1 \qquad\qquad\qquad\quad \text{for} \quad m = 1 \\ &k_T = 1, 2, \ldots\ldots\,. \end{aligned}$$

In this connection, in the reference 3), the behaviour of the change of v^{+0} have been represented by continuous functions, but the one should be done by the discrete functions as shown in Eq.s (19) to (21).

As Eq. (20) can be rewriten by

$$v_{k+1}{}^{+0} = v(k\tau) = v_\infty{}^{+0}(1 - \varepsilon^{-\frac{k\tau}{T}}) + v_1{}^{+0}\,\varepsilon^{-\frac{k\tau}{T}}\,, \tag{22}$$

we can see that the dynamic performance of the motor in Fig. 1 is equivalent to the one of the first order sampled data system as shown in Fig. 7, where the sampling

period is τ. The figure will be useful when we wish to find the frequency response of the motor.

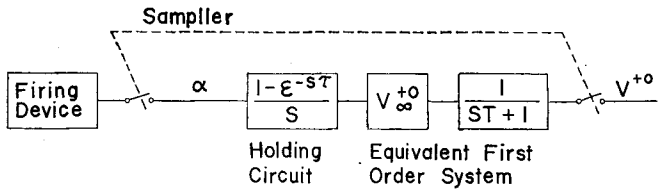

Fig. 7. Equivalent sampled data system of control circuit sketched in Fig. 1.

Next, with respect to the value of m, we can find one graphically from the $v^{+0}-\Delta v^{+0}$ curve for the given firing angle α. However, in the case when the motor rotates continuously as shown in Fig. 5(c), it is convenient that we look for the value of m in the following manner. As t_3 is the function of v^{+0} as seen in Eq. (14), we have

$$m = -\frac{d\Delta v^{+0}}{dv^{+0}} = -\left(\frac{\partial \Delta v^{+0}}{\partial t_3}\frac{dt_3}{dv^{+0}} + \frac{\partial \Delta v^{+0}}{\partial v^{+0}}\right). \tag{23}$$

Calculating $\partial \Delta v^{+0}/\partial t_3$ from Eq.s (14) and (15), we can obtain $\partial \Delta v^{+0}/\partial t_3 = x_4(t_4)\, i(t_3)/C = 0$. Consequently m can been expressed as follows:

$$m = -\frac{\partial \Delta v^{+0}}{\partial v^{+0}} = 1 - x_4(\tau - t_3)\, x_{322}(t_3)\,, \tag{24}$$

and is independent of α.

6. Numerical Calculations and Experimental Results

In the previous sections, we have presented a theoritical method, by which we can analyse the dynamic perfornamce of the motor control circuit in Fig. 1. So in this section, in order to investigate the appropriateness of our method, let us compare the results of the numerical analysis with the experimental results, and also add some new suggestions to the speed control technique of the motor by the thyristor circuit.

6.1 Experimental Circuit.

Fig. 8 shows the schematic diagram of the experimental circuit, in which the firing angle of the thyristor T_h is controlled by the firing device, and the load of the motor M is adjusted by changing the load resistor R_e of the generator G_e. The revolving speed of M is measured with a tachometer generator T_g.

Table 1 presents the specification of the servomotors which are used for both M

and G_e, and Table 2 the values of circuit parameters, where we assume that the impedance of the transformer T_r and the forward resistance of T_h are neglegible.

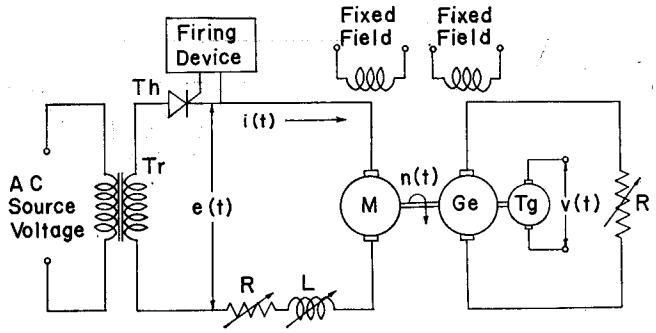

Fig. 8. Schematic diagram of experimental circuit.

Table 1. Specification of the dc servomotor.

Type (maker)	TD13-5 (Sanyo Electric Co.)
Rated power	200 W
Rated voltage	100 V
Rated current	2.7 A
Rated speed	3000 rpm
Rated field current	250 mA

Table 2. Circuit parameters.

Mechanical parameters	Electric parameters
J = 0.00214 kg · m Q_s = 0.263 N · m Q = 0.168 N · m F = 0.000364 to 0.0299 N · m · s/rad	C = 14.0 mF I_s = 0.672 A I_q = 0.430 A G = 2.38 to 195.6 m℧
K_v = 0.391 V · s/rad K_t = 0.391 N · m/A	E_m = 141.4 V f = 60 Hz R = 14.1 Ω L = 6.3, 46.9, 108.7 mH

6.2 Steady State Characteristics.

Fig. 9 shows the calculated relations between α and V_d for the following values of L and G, i.e.

L=6.3, 46.9, 108.7 mH,

G=2.38, 20.9 $m\mho$,

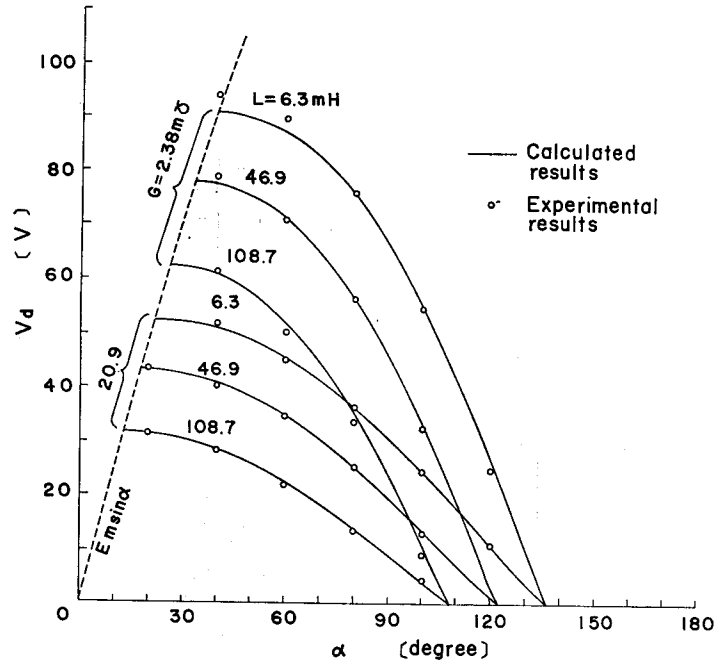

Fig. 9. Relation between α and V_d.

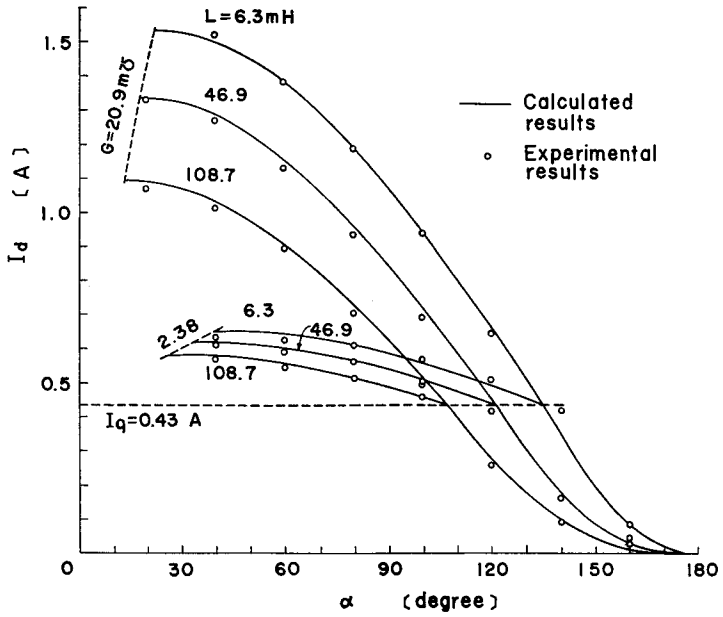

Fig. 10. Relation between α and I_d.

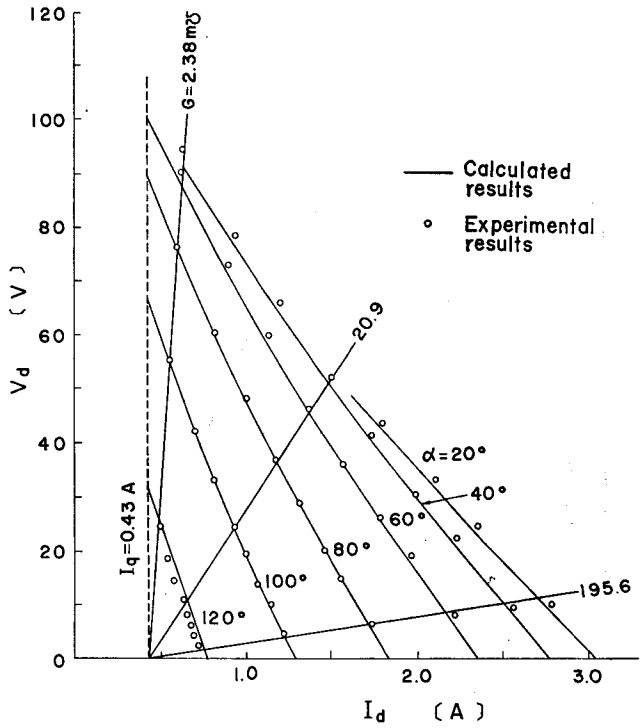

Fig. 11. Relation between I_d and V_d for L=6.3 [mH].

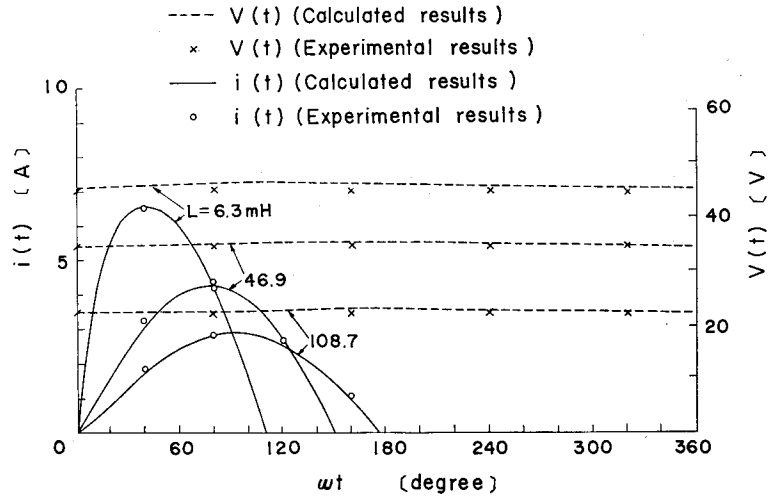

Fig. 12. Instantanuous waveforms of $i(t)$ and $v(t)$ for G=20.9 [$m℧$] and α=60°.

and Fig. 10 the ones between α and I_d. In these figures some experimental results are marked, too.

Now, when the generated torque $K_t I_d$ exceeds the coulomb friction torque Q, i.e. $I_d \geq I_q$, and in other words the motor rotates continulusly, the values of V_d and I_d have been calculated by Eq.s (16) and (17). On the other hand, in the case when α increases and I_d becomes smaller than I_q, namely we can assume that the motor is resting, the value of I_d has been evaluated by Eq. s(11). Next, when α becomes too small to satisfy $E_m \sin \alpha > V_d$, the thyristor can't be fired and the circuit performance becomes unstable.

In Fig. 11 the calculated $I_d - V_d$ curves, corresponding to the speed characteristic ones, are presented and also some experimental results are plotted. From the figure we can see that V_d for a specific firing angle decreases steeply according to the increase of I_d. We think that this is owing to the resistance voltage drop RI_d and the decrease of the terminal voltage E_d in Eq.s (17).

Fig. 12 shows the examples of instantanuous waveforms of $i(t)$ and $v(t)$ at $\alpha = 60°$. From the figure we see that the fluctuation of the motor speed is neglegible, because our dc motor has a large value of inertia moment as shown in Table 2. Furthermore, when the value of L increases, the conducting duration of $i(t)$ increases but the values of $i(t)$ and $v(t)$ decreases.

Next comparing the theoretical results in the steady state with the experimental ones in Fig.s 9 to 12, we see that good agreement is obtained. The difference between both results is surmised to be caused by the armature reaction of the motor, the nonlinearities of circuit parameters and the measurement errors.

Now the fluctuation of $v(t)$ is very small as seen in Fig. 12, so we can suppose that the conventional analysis, in which the motor speed is assumed to be constant, is available occasionally in the analysis of the steady state characteristic. As it is assumed that $v(t) = V_d$ is constant in the conventional method, so this method is convenient to analyse the relations among V_d, I_d, $i(t)$ and α. However the method is not useful to investigate what influence the circuit parameters C, G, I_q and etc. give the characteristics of the motor. Also the method can't be used for the analysis of the ones of the motor, of which the inertia moment is small and the fluctuation of the speed can't be neglected.

6.3 Transient Characteristics.

Fig. 13 shows the representative oscillogram of $e(t)$, $i(t)$ and $v(t)$ in the transient state.

In Fig.s 14 and 15 we plot some examples of the calculated relations between v^{+0} and Δv^{+0} and also show some experimental results, which are measured from the

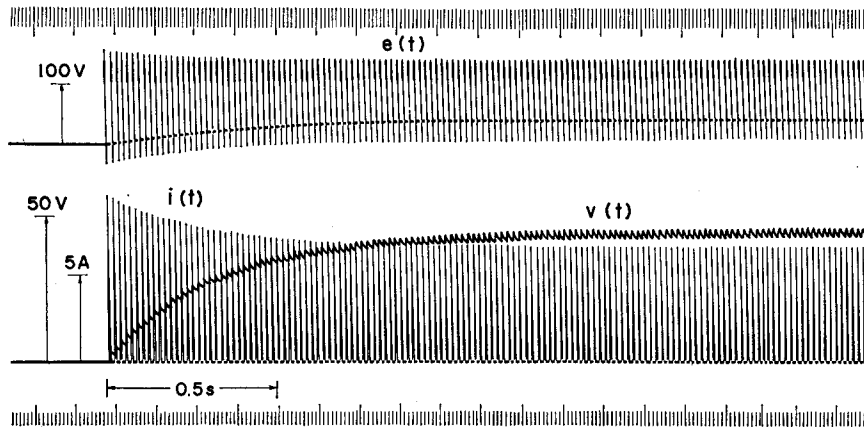

Fig. 13. Example of oscillogram of transient response.

oscillograms of $v(t)$. Comparing the calculated results with the experimental ones, fairly good agreement has been obtained.

As described in section 5, we can easily see the transient performance of the motor from the characteristic curves in Fig.s 14 and 15. In this connection, when v^{+0} exceeds $E_m \sin\alpha$, for example $E_m \sin 20° = 48.4V$, and the thyristor isn't fired, Δv^{+0} drops from the right end of the curve for $\alpha = 20°$ to the one for $\alpha = 180°$.

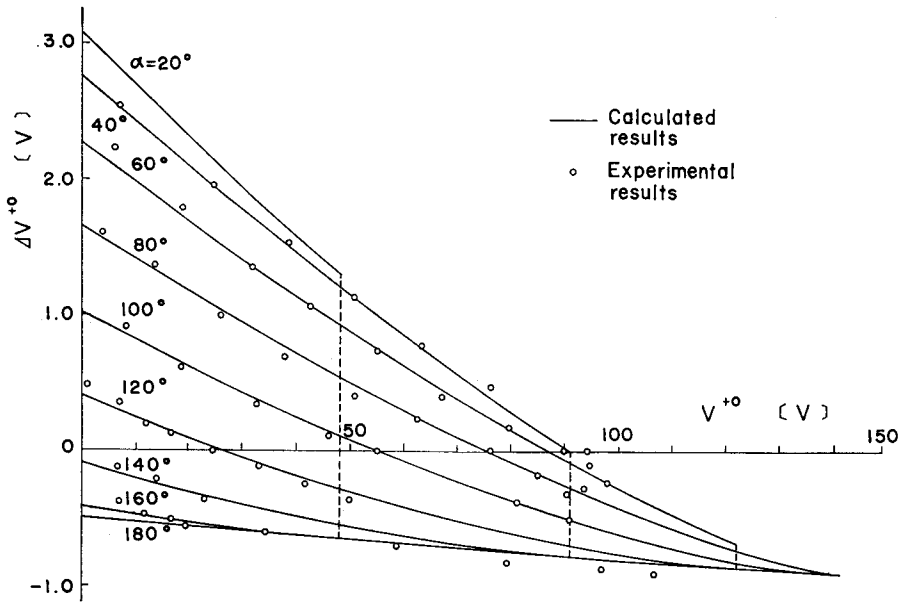

Fig. 14. Relation between v^{+0} and Δv^{+0} for $L=6.3$ [mH] and $G=2.38$ [$m\mho$].

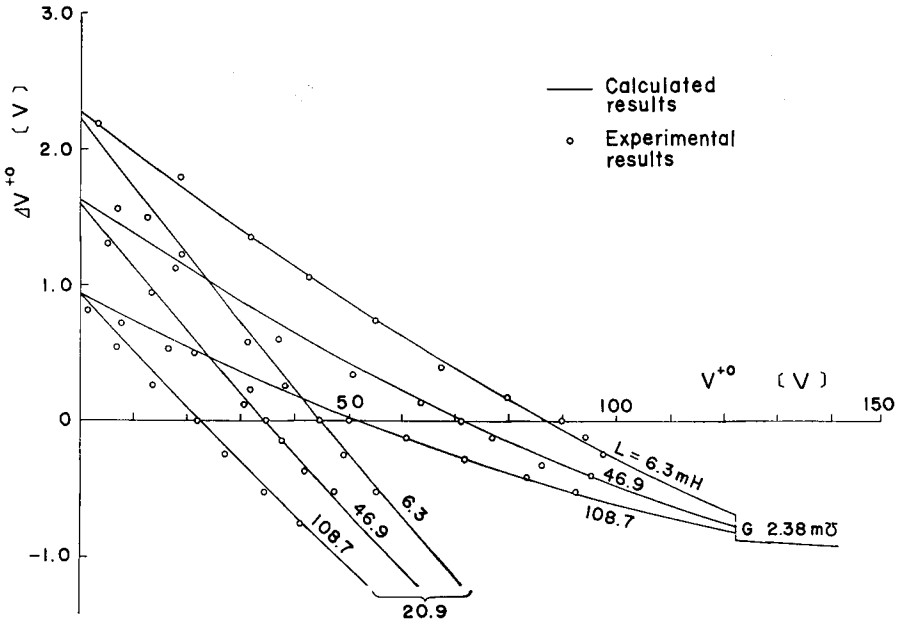

Fig. 15. Relation between v^{+0} and Δv^{+0} for $\alpha=60°$.

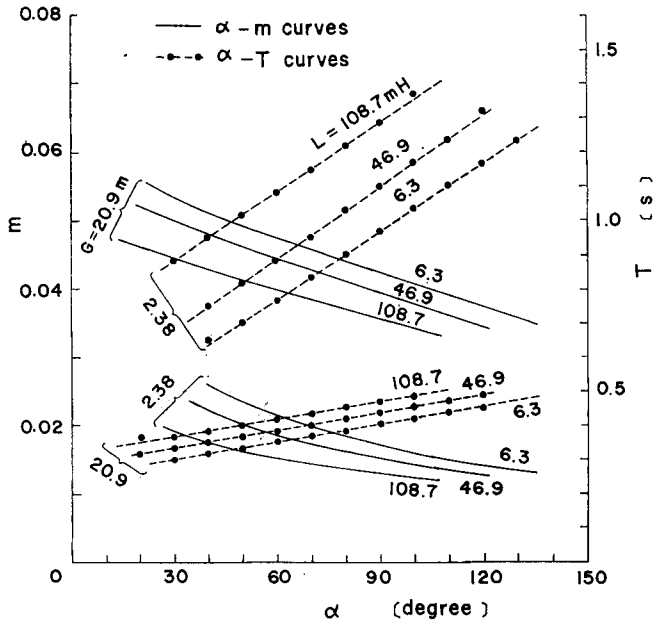

Fig. 16. Relation among α, m and T.

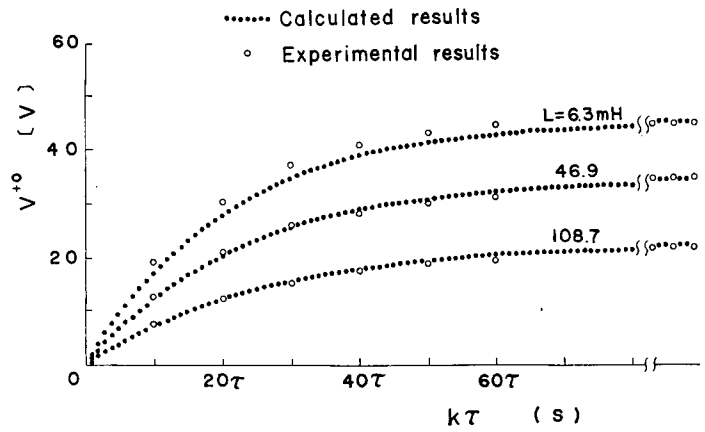

Fig. 17. Transient response of v^{+0} for $G=20.9$ [$m\mho$] and $\alpha=60°$.

In Fig. 16 we plot the values of m and T for $\Delta v^{+0}=0$, which are calculated from Eq.s (16), (21) and (24). From the figure we see that the values of m and T are much influenced by the value of G rather than the one of L, because the value of the mechanical time constant $J/F=C/G$ is much larger than the value of the electric one L/R for our motor. Next comparing the value of T plotted in Fig. 16 with the one of T_d given in Eq. (18), the former is several times larger than the latter, as, for example $T_d=0.191$ s for $G=2.38$ $m\mho$ or $T_d=0.152$ s for $G=20.9$ $m\mho$, because there can exist a duration when the armature current is blocked and the motor is decelerated, when the motor is driven by the thyristor rectifier circuit.

In Fig. 17 we plotted the calculated transient values of v^{+0} for $\alpha=60°$, which are found by putting the values of m or T obtained from Fig. 16 into Eq. (20) or Eq. (22), and the experimental ones which are acquired from the oscillograms of $v(t)$. It is seen that the calculated results agree with the experimental ones relatively well.

Next let us consider what influence the value of C gives the dynamic performance. Fig. 18 shows the calculated relations between v^{+0} and Δv^{+0} for some values of C and G. From the figure we see that the values of C have little influence on the initial voltage $v_\infty{}^{+0}$ in the steady state, but much on the behaviour of v^{+0} in the transient state. Therefore, when we wish to know the transient characteristics of the motor, we must measure exactly the values of C and G, i.e. J and F. On the other hand, we must know the exact one of G and L for the steady state characteristics.

As shown in Fig.s 14, 15 and 18, it can be seen that the $v^{+0}-\Delta v^{+0}$ curves are able to be fairly well approximated by the straight lines in spite of the values of L, G and C.

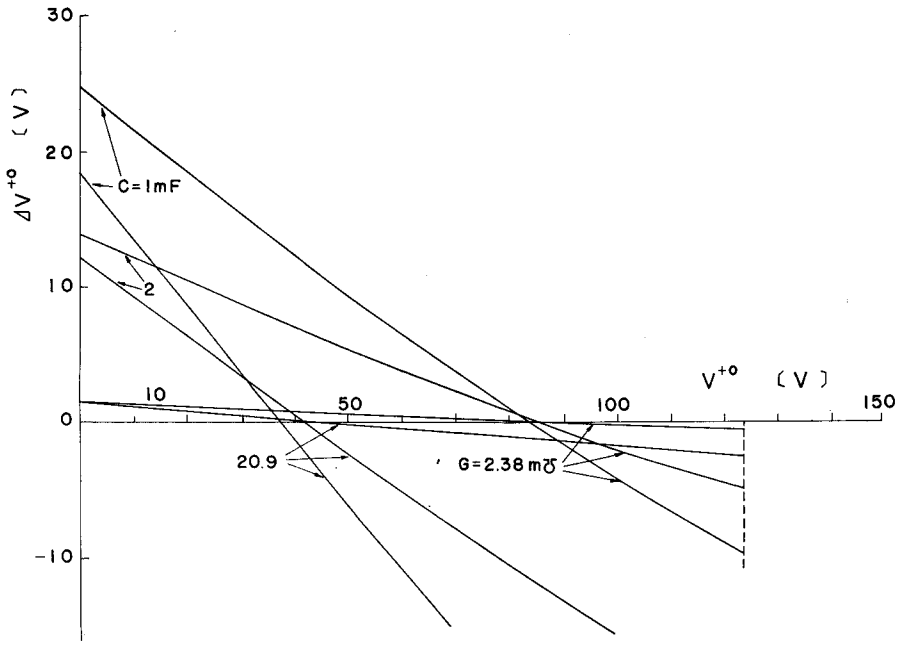

Fig. 18. Influence of the values of C and G on v^{+0}—Δv^{+0} curve for $L=6.3$ [mH] and $\alpha=60°$.

7. Conclusions

In this paper the authors have introduced a theoretical method to analyse the transient and steady state characteristics of a separately excited dc motor controlled by a single-phase half-wave thyristor rectifier circuit, and we have shown the appropriateness of this method by comparing the calculated results with the experimental ones, with respect to the transient and steady state performances of our circuit. Also, we have investigated the influences of the circuit parameters on the performance.

Now this theoretical method is applicable to analyse the dynamic characteristics of the motor controlled by polyphase rectifier circuits, chopper circuits and others, where the armature current is interrupted periodically. Especially the equivalent block diagram of the motor performance shown in Fig. 7 will be applicable to the analysis of the frequency response of the motor.

Acknowledgments

The authors wish to express their appreciation to Messrs. S. Okabayashi of

IBM Jaqan, K. Yano of Toshiba Elactric and Y. Morishita of Toyo Kogyo Companies for their help in the experiments and the digital computation, and to staff menbers of the center of the Digital Computor FACOM 230–60 at Kyoto University.

References

1) L. Dale Harris; AIEE Trans., **70,** 1582 (1951).
2) T. Takeuchi; "The Theory of SCR Circuits and its Applications to the Control of Motors," Ohm, 44 (1968).
3) K. Togino; J. Mech. Lab. J., **13,** 86 (1959).
4) S. Hayashi; "Periodically Interrupted Electric Circuits," Denki-Shoin, 79 (1961).
5) G. J. Thaler and W. A. Stein; AIEE Trans., **75,** 410 (1956).
6) A. Mogi; "Synchros and Servomotors," Nikkan Kogyo Newspaper Office, Tokyo, 111 (1966).